ACS ES&T Air

pubs.acs.org/estair

Article

Conversion of Catechol to 4-Nitrocatechol in Aqueous Microdroplets Exposed to O_3 and NO_2

Md Sohel Rana, Seth T. Bradley, and Marcelo I. Guzman*

Cite This: *ACS EST Air* 2024, 1, 80−91

Read Online

ACCESS | Metrics & More | Article Recommendations | Supporting Information

ABSTRACT: Catechol is a widespread atmospheric dihydroxybenzene present in vehicle emissions, biomass burning, and combustion pollution plumes. Although the daytime reactivity of catechol is controlled by ozone (O_3) and hydroxyl radicals (HO), the action of nitrate radicals (NO_3) on the surface of aqueous atmospheric particles should become significant at night. This work simulates nighttime interfacial chemistry between hydrated catechol and adsorbed NO_3 to form 4-nitrocatechol during experiments lasting ≤1 μs. Surface-sensitive online electrospray ionization mass spectrometry (OESI-MS) examines the reaction on the water surface under variable ratios of $[NO_2]$ and $[O_3]$. The produced 4-nitrocatechol is quantified by a standard addition in real-time experiments under $[NO_2]$:$[O_3]$ ratios of 1:1, 2:1, 3:1, and 4:1. Three mechanisms contribute to produce 4-nitrocatechol: (1) electron and proton transfers from catechol to NO_3, forming a semiquinone radical, (2) electrophilic NO_3 attack to the ring to yield a cyclohexadienyl radical intermediate, and (3) electrophilic attack to the ring by nitronium ion (NO_2^+) formed at the interface of water by colliding N_2O_5(g) at low pH. Ozonolysis competes strongly with nitration when using $[NO_2]$:$[O_3]$ ratios 1:1 or smaller. Instead, nighttime chemistry under higher molar ratios proceeds mainly by nitration with a maximum yield of 0.90 for $[NO_2]$:$[O_3]$ = 4:1.

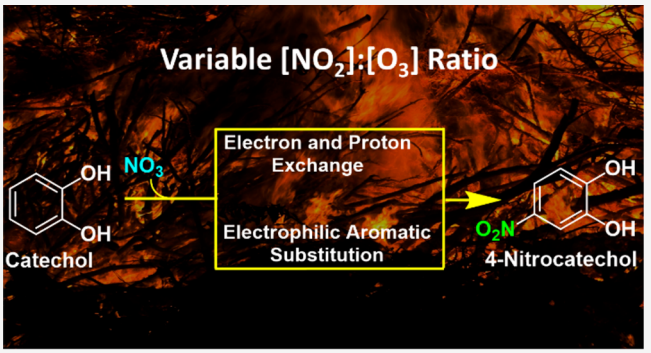

KEYWORDS: *phenols, dihydroxybenzene, nitrogen dioxide, ozone, nitrate radical, hydroxyl radical, secondary organic aerosol*

INTRODUCTION

Biomass burning and combustion emissions supply molecules of catechol to the atmosphere,[1−3] which acts as a multiphase precursor in the production of 4-nitrocatechol,[4−6] found in widespread atmospheric brown carbon.[7,8] A variety of nitroaromatic compounds and their phenol and catechol precursors have been identified in particulate matter and/or the gas phase of samples collected over (1) rural regions of Germany,[9] (2) the cities of Jinan, Xian, Hong Kong, and Beijing, China,[4,5,10] and (3) Detling, U.K.[11] The prevalence of nitroaromatic compounds was assigned to the secondary processing of vehicular exhaust, biomass burning, and fossil fuel combustion emissions,[4,5,10,11] where exposure to considerable levels of nitrogen dioxide (NO_2) occurs.[9] Biomass burning could dominate up to 60% of the production-catechol-derived nitroaromatic compounds detected both in the gas and particle phases during winter time in a rural site in China.[6]

The effective absorption of light by brown carbon can account for up to 48% of the overall radiative forcing of aerosols in the near UV and visible spectrum, demanding a better understanding of the chemistry generating nitroaromatic compounds.[7,12] Most of the previous studies of the oxidation of catechol by nitrate radicals (NO_3) described chemistry in the gas or aqueous phases to produce 4-nitrocatechol to make secondary organic aerosol,[13,14] with only one recent study that tackled the mechanism at the air−water interface.[15] However, the examination of the interfacial reaction under variable NO_2:O_3 molar ratios remains unexplored. As a polar and surface-active molecule, catechol partitions from the gas phase into aqueous atmospheric particles, where reactivity at the interface can proceed by quite unique pathways. The typical reactivity of phenols with NO_3, only available for comparison in the gas-phase, could be one-million to ten-million higher than for O_3.[16,17] Comprehensive mechanisms for the interfacial oxidation of catechol by O_3 and in situ produced $HO^\bullet$ showed the participation of semiquinone and cyclohexadienyl radicals.[18−21] Therefore, the participation of the previous intermediates should also contribute to the efficient nighttime production of 4-nitrocatechol at the air−water interface of particles containing catechol that are exposed to NO_3.

Received: June 21, 2023
Accepted: September 28, 2023
Published: November 29, 2023

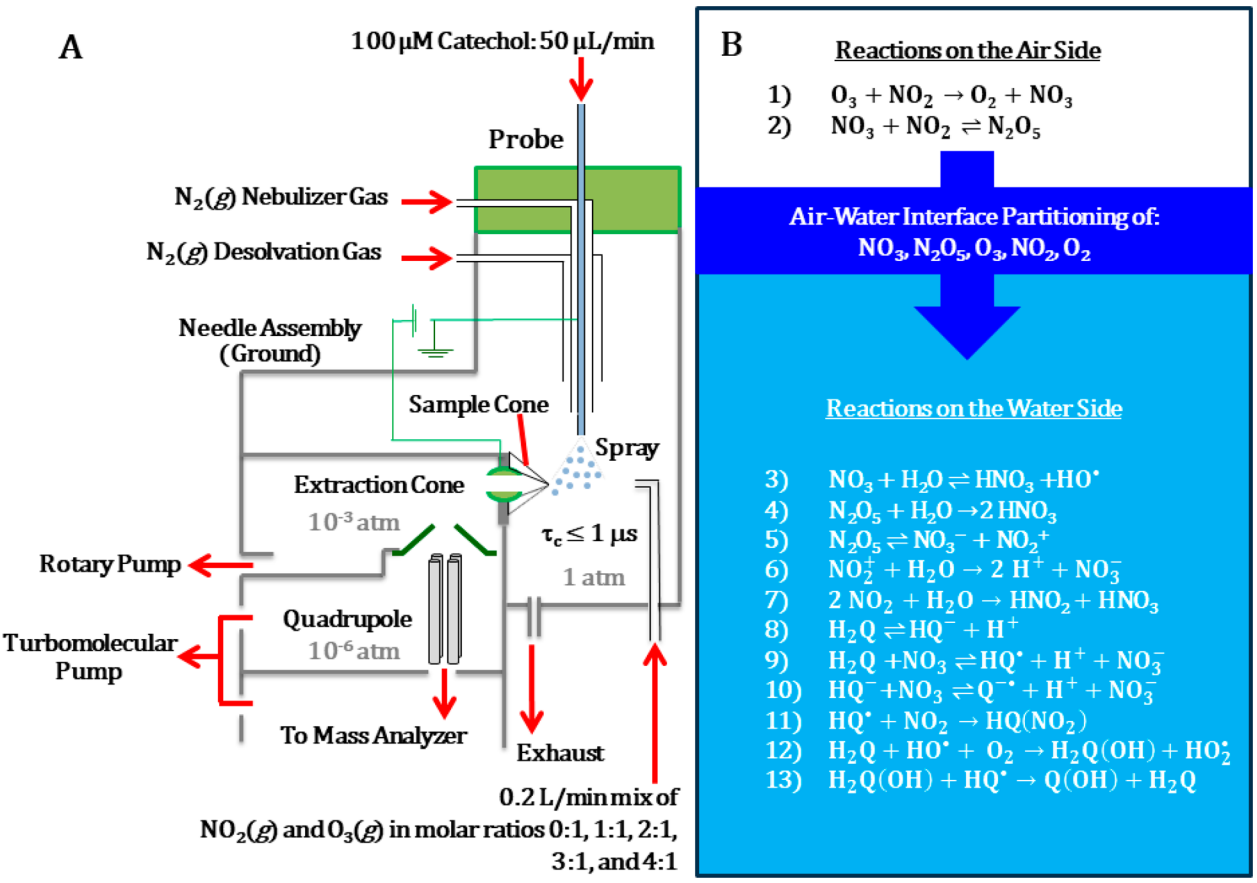

Figure 1. (A) Illustration of the online electrospray ionization mass spectrometry (OESI-MS) reactor. (B) Summary of key interfacial reactions registered on the water side of the interface with air (in the light-blue box) that are discussed in detail in the text.

This work examines the oxidation of catechol by NO_3 at the surface of aqueous microdroplets by using surface-sensitive online electrospray ionization (OESI) mass spectrometry (MS). OESI-MS has an ultra-fast contact time, $\tau_c \leq 1$ μs, and a detection time $\tau_d = 1$ ms,[3,18,19,22−24] which allow the investigation of this oxidation under relevant conditions for understanding the chemistry occurring in atmospheric waters. Our previous work with this setup reported two mechanistic schemes for the nitration of catechol,[15] which are initiated by electron transfer or direct NO_3 attack to the ring. In this work, we carefully study how the variation of relative NO_2:O_3 molar ratios can enhance the formation of 4-nitrocatechol, which is quantified in the surface layer by a method of standard addition. The OESI-MS experiments below exposing catechol for the first time to variable molar ratios of O_3 and NO_2 monitor the formation of 4-nitrocatechol and reveal processes that can worsen the pollution from biomass burning and combustion emissions.

EXPERIMENTAL METHODS

Sample Preparation. A 100 μM catechol (Sigma-Aldrich, 99.9%) solution was freshly made daily in degassed ultrapure water (Elga PURELAB Flex, 18.2 MΩ·cm^{-1}). The work verified that the purity of catechol was maintained by registering the ultrahigh pressure liquid chromatogram with a reversed phase C18 column, which verified the reagent appeared alone in the chromatogram. If needed, the pH of the solution was adjusted with dilute HCl (EMD Millipore, 37.67%) and/or dilute NaOH (AMRESCO, ≥97%) solutions.

The concentration selected for this work is justified in the partitioning of 5−50 ppbv catechol detected over biomass burning plumes[25] onto aqueous particles. Based on the Henry's law constant of catechol, H_0 = 4600 M atm^{-1},[26] predicted equilibrium concentrations fall in the range 22−223 μM. Thus, the selected 100 μM concentration fall in the center of the predicted range for atmospheric aqueous particles. Furthermore, experiments in the pH range from 4 to 8 are specifically relevant to cloud water (pH 3−8), and a large interval of environmental aerosol particles (pH 1.5−7.7).[15,27]

OESI-MS Setup. The 100 μM catechol solution was pneumatically aerosolized into the OESI−MS at 50 μL/min (Figure 1).[23,28] The instrument provides an ambient pressure (1 atm) flow through reactor that enables the nitration study at the surface of a mist of generated aqueous microdroplets in $\tau_c \leq 1$ μs and a $\tau_d = 1$ ms detection time as described before.[3,15,18,19,23,24,28]

The conditions for this type of experiments with catechols have been previously optimized[15,18,19] at 70 psi for the nebulizer pressure, −1.9 kV for the nebulizer voltage, and −50 V for the cone voltage. Mass spectra acquired for at least 30 s represent the normalized ion count values ($I_{m/z}$) for the largest anion mass-to-charge ratio (m/z^-) in the spectrum, unless indicated otherwise. The solvent was background-subtracted from all mass spectra, which were collected in duplicate experiments. Previous work discarded any possible solvent evaporation contribution to the interfacial reactions studied due to the large size of aqueous microdroplets produced in this setup and the ultrafast contact time ($\tau_c \leq 1$ μs).[3,15,18,19,22,23]

https://doi.org/10.1021/acsestair.3c00001
ACS EST Air 2024, 1, 80−91

Similarly, the flow-through reactor was demonstrated to discard diffusion limitations,[18,19] The formation of clusters is minimized by the extra-soft conditions that also prevent ionization of gas phase molecules for contributing to the interfacial reactions reported.[3,18,19,23] Furthermore, appropriate controls verify the products are only the result of interfacial reactions.[3,15,18,19,23,24,28] For the quantification of 4-nitrocatechol (TCI America, 99.9%), the method of standard addition was used during the oxidation experiments. Such quantification was performed to increase the intensity of the peak at m/z^- 154 by 1−4 times after spiking relative to the unspiked peak. For this purpose, 100 μM catechol solutions were aerosolized and oxidized unspiked, and after spiking, they were subjected to a final concentration of 25, 50, or 250 nM 4-nitrocatechol.

The OESI-MS reactor for probing fast oxidations at the air−water interface has been carefully described before.[28] Briefly, the use of OESI-MS in the present experiments allows us to specifically target the study of interfacial reactions described in four steps: (1) oxidation reactions occur during the early stage of aerosolization, right upon the uptake of NO_3(g) molecules on the microdroplet's interface containing catechol. (2) The original microdroplets where the reactions occurred undergo evaporation accompanied by fission in smaller droplets. These resulting smaller droplets undergo charge crowding until repulsion overcomes the surface tension. (3) Anions are then produced from the latest progeny droplets, which continue undergoing desolvation and eventually reach the detector. Thus, the ions detected are ejected from the microdroplet's surface as the charge builds up, making the experiment surface-sensitive.[3,15,18,19,22−24,28] Solvent molecules and species in the gas-phase do not reach the analyzer because they are pumped away in the intermediate vacuum stage between the OESI probe and the MS. (4) The lower pressure orifice of the entrance cone attracts the ions created, which once in this sector continue traveling through the lower pressure entrance capillary toward the quadrupole mass analyzer. Furthermore, the surface-sensitive ability of our OESI-MS has been validated by detecting the same products during in situ studies with catechol, syringaldehyde, vanillin, and 4-hydroxybenaldehyde under a $\tau_c \leq 1$ μs and after analysis of surface reactions lasting from minutes to several hours.[18,20,28,29]

Production of Reactive Species. To produce reactive species, a dry flow of ozone (O_3) was mixed with dry nitrogen dioxide (NO_2) at fixed molar ratios. A flow of O_3(g) was prepared with a spark discharge O_3 generator (Ozone Solutions) fed with 0.50 L min^{-1} O_2 (Scott-Gross, UHP) provided a flow of O_3(g). The O_3 flow was diluted to the desired concentration, using 0.10−2.0 L min^{-1} N_2 (Scott-Gross, UHP), registered by UV spectroscopy at λ = 250 nm with a photodiode array (PDA) spectrometer (Thermo Evolution Array) in a quartz cuvette with a path length of 10.0 cm. Cylinders of NO_2 of 100, 200, or 214 ppmv (Scott-Gross, UHP, nitrogen balance) provided a 0.060 to 1.0 L min^{-1} flows to a 4.0 L amber flask, where mixing with O_3(g) enabled reaction R1 and equilibrium R2 to occur:

$$O_3(g) + NO_2(g) \rightarrow O_2(g) + NO_3(g) \quad (R1)$$

$$NO_3(g) + NO_2(g) \rightleftharpoons N_2O_5(g) \quad (R2)$$

producing NO_2:O_3 mixtures at fixed molar ratios 0:1, 1:1, 2:1, 3:1, and 4:1. After ≥30 min of equilibration, 0.20 L min^{-1} flow of the mixture was transferred through a short tube to the OESI-MS reactor, where final 61× dilution took place by the N_2(g) nebulizing gas (12.0 L min^{-1}).

RESULTS AND DISCUSSION

Assessment of Reactive Species Produced. Figure 2 displays examples of the absorbance spectra of reactive

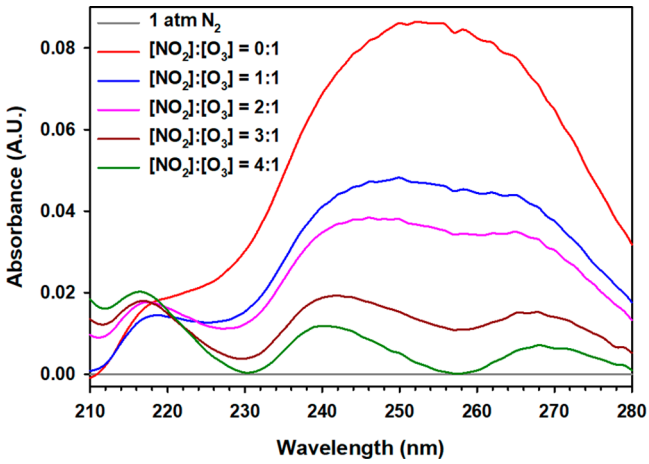

Figure 2. UV spectra of 0.20 L min^{-1} flow of (gray trace) 1 atm of N_2(g), (red trace) 31.8 ppmv of O_3(g), (blue trace) 31.8 ppmv of O_3(g) and 30.9 ppmv of NO_2(g), (pink trace) 31.8 ppmv of O_3(g) and 64.2 ppmv of NO_2(g), (brown trace) 31.8 ppmv of O_3(g) and 92.7 ppmv of NO_2(g), and (green trace) 31.8 ppmv of O_3(g) and 128.4 ppmv NO_2(g). The prepared ratio [NO_2]:[O_3] in the legend is provided for reference, as discussed in the text.

mixtures of [NO_2]:[O_3] prepared at molar ratios of 0:1, 1:1, 2:1, 3:1, and 4:1. In these experiments, the molar ratio of O_3 was fixed at 31.8 ppmv, and the variable molar ratio of NO_2 was 0, 30.9, 64.2, 92.7, and 128.4 ppmv. The concentrations of O_3 were retrieved from Figure 2 and reported in Table 1 based on the absorbance reading at λ = 250 nm using Beer's law with an absorption cross section ($\sigma_{250\ nm}$ = 1.1 × 10^{-17} cm^2 molecule^{-1})[30] for O_3 and a path length of 10.0 cm of the cuvette. Table 1 lists the experimental values for the input ratios of [O_3] and [NO_2] that enter the 4 L mixing amber flask together with the determined amount of [O_3] consumed by reaction R1, the calculated NO_3 production rate (P_{NO_3}), the time integrated [NO_3] generated, and the effective [NO_3]$_{eff}$ that impinges the surface of aqueous microdroplets after a 61× dilution with the N_2 nebulizing gas. For example, an absorbance reading A_{250nm} = 0.0861 before adding NO_2 (red trace in Figure 2) corresponds to [O_3] = 7.83 × 10^{14} molecules cm^3 (≡31.8 ppmv).

The O_3 output concentration after mixing (Table 1) was determined down the gas transmission line by the same absorption spectroscopy and enabled the assessment of the NO_3 production rate (P_{NO_3}) by eq 1:[31]

$$P_{NO_3} = k_{NO_3}[O_3][NO_2] \quad (1)$$

where k_{NO_3} = 3.2 × 10^{-17} cm^3 molecule^{-1} s^{-1} is the rate constant of reaction R1 at room temperature.[31] The rate constants for the forward and backward directions of equilibrium R2 at room temperature are $k_{N_2O_5}$ = 6.7 × 10^{-12} cm^3 molecule^{-1} s^{-1} and k_{NO_3} = 2.2 × 10^{-1} s^{-1}, respectively.[30] For [O_3] and [NO_2], one needs to calculate P_{NO_3} with eq 1,

https://doi.org/10.1021/acsestair.3c00001
ACS EST Air 2024, 1, 80−91

Table 1. Prepared Ratio $[NO_2]$:$[O_3]$, $[O_3]$, and $[NO_2]$ Input to Mixing Flask, $[O_3]$ Output After Mixing, $[O_3]$ Consumed, NO_3 Production Rate (P_{NO_3}), $[NO_3]$ Generated During 8.77 s Production Time with 3.0% Efficiency, Effective $[NO_3]_{eff}$ Impinging Aqueous Microdroplets after 61× Dilution with Nebulizer, and Output Ratio of $[NO_3]_{eff}$:$[O_3]_{out}$

$[NO_2]$:$[O_3]$	$[O_3]$ input[a]	$[NO_2]$ input[a]	$[O_3]$ output[a]	$[O_3]$ consumed[a]	P_{NO_3}[b]	$[NO_3]$ generated[a]	$[NO_3]_{eff}$[a]	$[NO_3]_{eff}$:$[O_3]_{out}$
0:1	7.83×10^{14}	0	7.83×10^{14}	0	0	0	0	0:1
1:1	7.83×10^{14}	7.61×10^{14}	4.38×10^{14}	3.45×10^{14}	3.80×10^{12}	9.90×10^{11}	1.62×10^{10}	2.3×10^{-3}:1
2:1	9.68×10^{13}	2.09×10^{14}	5.96×10^{13}	3.72×10^{13}	4.43×10^{10}	1.11×10^{10}	1.82×10^{8}	1.9×10^{-4}:1
2:1	3.88×10^{14}	7.64×10^{14}	1.82×10^{14}	2.06×10^{14}	1.36×10^{12}	3.43×10^{11}	5.62×10^{9}	1.9×10^{-4}:1
2:1	7.83×10^{14}	1.58×10^{15}	3.45×10^{14}	4.37×10^{14}	6.12×10^{12}	1.59×10^{12}	2.61×10^{10}	4.6×10^{-3}:1
3:1	7.83×10^{14}	2.28×10^{15}	1.39×10^{14}	6.44×10^{14}	1.33×10^{13}	3.46×10^{12}	5.66×10^{10}	2.5×10^{-2}:1
4:1	7.83×10^{14}	3.16×10^{15}	4.72×10^{13}	7.36×10^{14}	1.73×10^{13}	4.51×10^{12}	7.40×10^{10}	9.61×10^{-2}:1

[a]In units of molecules cm^{-3}. [b]in units of molecules cm^{-3} s^{-1}.

and a reliable approximation is to consider the amount of $[O_3]$ consumed by the addition of NO_2. This reacted concentration was obtained from a UV-visible measurement at λ = 250 nm before and after mixing with NO_2 and is listed in Table 1 as $[O_3]$ consumed. The $[NO_3]_{eff}$ acting on the surface of the microdroplets is provided by integration of P_{NO_3} during the residence time (t_r = 8.77 s)[32,33] the molecules of O_3 and NO_2 spend in the quartz cuvette before the mixture is transferred to the final PTFE line directing the flow to the OESI-MS system.

Additionally, it is fundamental to consider the wall losses of NO_3 by reaction R3 inside the quartz cuvette and the PTFE transfer line (the last reactors where NO_3 is produced by reaction R1) to the OESI-MS system:[32,34]

$$NO_3 \rightarrow \text{walls} \quad \text{(R3)}$$

The cuvette made of quartz ($k_{R3} \simeq 0.11$ s^{-1})[32,33] has a transmission efficiency of 3.5%.[15] The O_3 and NO_2 mixture is transferred through a PTFE line from the PDA to the surface of the microdroplets in 18.77 s.[15] The resulting wall loss[35] in this PTFE ($k_{R3} = 7.1 \times 10^{-3}$ s^{-1})[36] line proceeds with a transmission efficiency of 86.0%. Thus, the overall transmission efficiency for the produced NO_3 to reach the microdroplets' surface is 3.5% × 86.0% = 3.0%, which is applied to calculate $[NO_3]$ generated, listed in Table 1.

Table 1 also reports the effective $[NO_3]_{eff}$ that reacts with catechol on the microdroplets' surface by including the 61× dilution with the N_2 nebulizing gas. It is important to recognize that a uniqueness of this surface-sensitive OESI-MS system as a flow-through reactor is to facilitate monitoring the nitration of the catechol ring with the $[NO_3]_{eff}$ without further wall losses.[15] Finally, the wall loss of NO_3 can be taken as an upper limit to those of N_2O_5 because measurements in a fluorinated ethylene propylene reactor indicate that the loss of NO_3 ($k_{wall} = 1.6 \times 10^{-3}$ s^{-1}) proceeds ~5× faster than N_2O_5 ($k_{wall} = 3.28 \times 10^{-4}$ s^{-1}).[37]

Polluted regions affected by biomass burning typically display ranges of $[O_3] = 2.0 \times 10^{12}$ to 4.9×10^{12} molecules cm^{-3} (80−200 ppbv) and $[NO_2] = 1.2 \times 10^{12}$ to 2.5×10^{12} molecules cm^{-3} (50−100 ppbv).[38−43] In such situations, the likely $[NO_3] = 1.2 \times 10^{8}$ molecules cm^{-3} (≡5 pptv) in a biomass burning plume[44] is close to the low end $[NO_3]_{eff}$ in Table 1, but exceeded by ~10^2× by most values. While many $[NO_3]_{eff}$ values in Table 1 appear high compared to field measurements, the experiments are needed to perform this laboratory work and facilitate fundamental information that reveals natural mechanisms of nitration in the environment described in the next section.

Production of 4-Nitrocatechol on the Surface of Aqueous Microdroplets. The reaction of NO_3 with catechol on the surface of the microdroplets is monitored at reported m/z^- values without wall losses due to the flow-through nature of this surface-sensitive OESI-MS reactor.[18,19,22−24] The bottom panel of Figure 1 displays the OESI-MS spectra of 100 μM catechol exposed to a 0.20 L min^{-1} of 1 atm of N_2(g), where catechol ($C_6H_6O_2$, MW 110) loss of a H^+ proton generates the anion ($C_6H_5O_2^-$) observed at m/z^- 109. Upon reaction of the catechol ring with an effective O_3 molar ratio of 521 ppbv (experiment for a ratio $[NO_2]$:$[O_3]$ = 0:1), the expected hydroxylation products, hydroxyquinone and trihydroxybenzene, at m/z^- 123 ($C_6H_3O_3^-$) and m/z^- 125 ($C_6H_5O_3^-$), respectively, are registered in the mass spectrum as small peaks.[18,19] The two panels at the bottom verify that in the absence of NO_2 in the mix with O_3, catechol does not produce its nitroaromatic product. For a ratio $[NO_2]$:$[O_3]$ = 1:1, when 509 ppbv NO_2 is added to 521 ppbv O_3, in addition to detecting the parent peak for catechol at m/z^- 109, the nitrate ion (NO_3^-) at m/z^- 62 is detected with an intensity of 93%.

One origin of the NO_3^- product at m/z^- 62 is the hydrolysis of NO_3 or N_2O_5,[45,46] although it can also be formed by electron transfer from catechol to NO_3.[15] Outstandingly, the fourth largest peak in the mass spectrum for the 1:1 ratio in Figure 3 appears at m/z^- 154, which corresponds to the formation of 4-nitrocatechol from the reaction of catechol with NO_3. The small peak at m/z^- 124 is an expected fragment from collisional-induced dissociation of the parent 4-nitrocatechol anion at m/z^- 154.[15] The small peaks at m/z^- 123 and 125 from hydroxylation of catechol by in situ generated $HO^\bullet$ are still observed in the mass spectrum.[18] Finally, the third largest peak in the spectrum at m/z^- 147, with a normalized ion count of 16.4%, is assigned to dihydroxymaleic acid or its isomer, dihydroxyfumaric acid. Clearly, the intensities of the two key products, 4-nitroctaechol (m/z^- 154) and NO_3^- (m/z^- 62), grow as the ratio of $[NO_2]$:$[O_3]$ approaches 4:1 (toward the top of Figure 3).

OESI-MS only detects products from the interfacial reaction of catechol positioned on the outermost layers of the aqueous microdroplets. The oxidizer uptake onto the water surface must occur first for catechol to react and later detect the ions.[3,18,19,23] The ultrafast dynamics and geometric arrangement of this system with a nebulizer gas velocity about ~1200-times larger than the infused liquid velocity and the 61-times lower flow of oxidizer than nebulizer gas discard the possible observation of products from gas-phase reactions. In other words, such hypothetical gas-phase products cannot be

https://doi.org/10.1021/acsestair.3c00001
ACS EST Air 2024, 1, 80−91

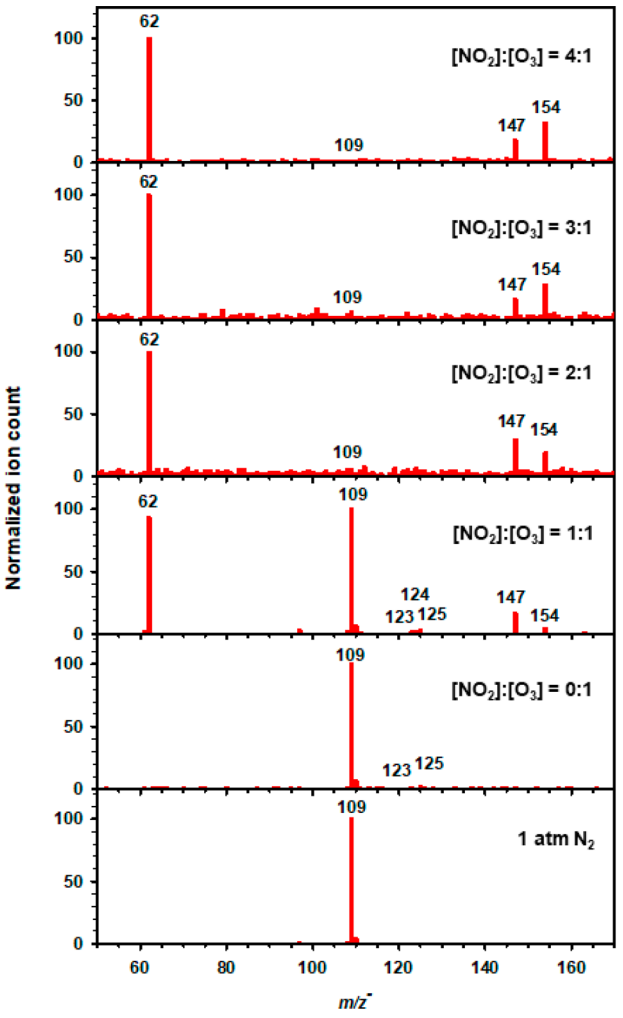

Figure 3. Online electrospray ionization mass spectra of 100 μM (bottom) catechol (m/z^- 109) reacting with (from bottom to top) 1 atm N_2, and $[NO_2]$:$[O_3]$ ratios (oxidizer concentrations input of 7.83 $\times$ 10^{14} molecules of O_3 per cm^3 in Table 1) of 0:1, 1:1, 2:1, 3:1, and 4:1. Ion count values ($I_{m/z}$) are normalized percentages relative to the largest ion in the spectrum, representing 100%.

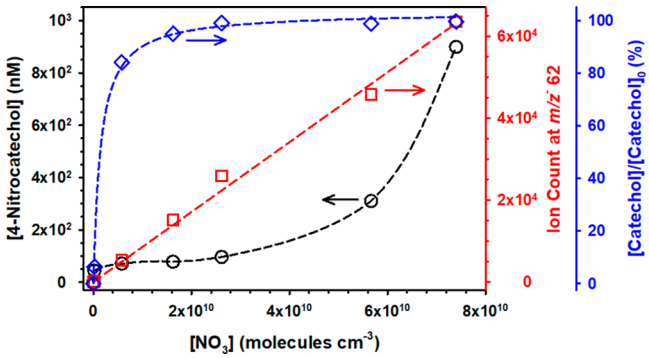

Figure 4. Normalized consumed catechol during oxidation ([catechol]/[catechol]$_0$) (blue diamond), and production of 4-nitrocatechol (black circle) and ion count for nitrate ion production at m/z^- 62 (red square).

readsorbed to the water surface (needed for charge creation). Furthermore, no ions for assigned products are detected in the absence of either water, catechol, or the oxidizer. Thus, the 4-nitrocatechol gas-phase production in our system would remain undetected. A summary of the key reactions registered in the water side of the interface in this work is provided in Figure 1B. The top part of Figure 1B with a white background displays the reactions of NO_3 and N_2O_5 formation in the gas-phase, while the center part with the arrow in blue color symbolizes the partitioning through the air water-interface of all the gases in an experiment. The bottom box in Figure 1B with a light-blue background shows the reactions occurring on the water side of the interface.

An explanation of the effect of variable $[NO_2]$:$[O_3]$ ratios is presented for the first time below for the interfacial nitration of catechol. The effect of pH in the range of 4−10 is known to favor the formation of 4-nitrocatechol under strong acidic conditions.[15] Figure 4 shows in blue diamonds the percentage of catechol consumed during oxidation relative to the value before addition of oxidizer ($100 - I_{109}/I_{109,0}$) corresponding to increasing $[NO_3]_{eff}$. The consumed catechols is cautiously fitted with the hyperbola $[Cat]/[Cat]_0 = 103.3\ [NO_3]_{eff}/(1.65 \times 10^9$ molecules $cm^{-3} + [NO_3]_{eff})$ with a coefficient of determination $r^2 = 0.9851$. The plateau of this fitted curve quickly reaches ∼100% (full consumption) in less than a microsecond if there are enough NO_3 molecules to react with all of the interfacial catechol available. Thus, under the working conditions with 100 μM catechol, the consumption of the organic probe upon reaction with NO_3 should proceed to a 50% for a predicted $[NO_3]_{eff} = 1.65 \times 10^9$ molecules cm^{-3} (≡ 66.8 pptv).

In this system, and even though catechol is continuously replenished to the interfacial region, the precursor for organic nitrate formation is still completely consumed for the $[NO_2]$:$[O_3]$ = 2:1, 3:1, and 4:1 values examined in Figures 2 and 3. The products observed by OESI-MS are only those from interfacial reactions on the outermost layers of the aqueous microdroplets between catechol and the dissolved reactive gases, which precedes the formation of ions detected.[3,18,19,23] Figure 4 also depicts the efficient production of several hundred nanomolar 4-nitrocatechol (black circles). 4-Nitrocatechol only appears for $[NO_2]$:$[O_3]$ = 1:1, and rapidly increased for a ratio ≥2:1 (as all interfacial catechol is consumed by $[NO_3]_{eff} > 2.61 \times 10^{10}$ molecules cm^{-3}). Finally, it is evident in Figure 4 that the interfacial production of nitrate ions increases linearly for higher oxidizer concentration as $I_{62} = 8.53 \times 10^{-7}$ cm^3 $molecules^{-1}$ $[NO_3]$.

The hyperbolic shape of the plot of consumed catechol (%) vs concentration of oxidizer (blue diamonds) in Figure 4, obtained from the relative ion counts at m/z^- 109 with and without oxidizer ($I_{109}/I_{109,0} \times 100$), resembles a Langmuir−Hinshelwood-type of dependence that supports the experiments that have evaluated reactions at the air−water interface. Based on the shape of Figure 4, the formation of 4-nitrocatechol starts as soon as NO_3 is created, but cannot account for all the consumed catechol, as other products can be generated (e.g., dihydroxymaleic acid). The curves for consumed catechol and produced 4-nitrocatechol in the range of $[NO_3]_{eff}$ depicted in Figure 4 resemble each other, but their differences are simply due to the generation of other products. The production of nitrate ion registered in Figure 4 must be related to several heterogeneous processes, such as the hydrolysis of adsorbed NO_3 (reaction R4) and N_2O_5 (reaction R5) on the microdroplets' surface that create HNO_3 ($pK_{a,HNO_3} = -1.38$):[45,47−49]

https://doi.org/10.1021/acsestair.3c00001
ACS EST Air 2024, 1, 80−91

$$NO_3(ads) + H_2O(l) \rightarrow HNO_3(aq) + HO^{\bullet}(aq) \quad (R4)$$

$$N_2O_5(ads) + H_2O(l) \rightarrow 2HNO_3(aq) \quad (R5)$$

Reaction R5 consumes ~20% of N_2O_5 molecules colliding with the microdroplets' surface.[50] Indeed, reactions R4 and R5 acidify the surface when the $[NO_2]$:$[O_3]$ mixture partitions onto the surface of microdroplets. This chemistry also contributes to explaining the observation of nitrate ion in particulate matter exposed to high $[NO_x]$.[51] The Henry's law constants of NO_3 and N_2O_5 in water at room temperature have been estimated to be $H_{0,NO_3} = 0.2\ (\pm 0.1)$ M atm^{-1} and $H_{0,N_2O_5} = 8.81 \times 10^{-2}$ M atm^{-1}, respectively.[45,52,53] A modeling study suggests that adsorption on the surface of water is the key limiting step of reaction R5[54] as a sink for N_2O_5, which is most favorable at low pH.[55−57] Partitioning of unreacted gaseous NO_2 (from the mixture) into water can occur with a Henry's law constant $H_{0,NO_2} = 7.0 \times 10^{-3}$ M atm,[58] by reaction R6:

$$2NO_2(ads) + H_2O(l) \rightarrow HNO_2(aq) + HNO_3(aq) \quad (R6)$$

dropping the surface pH through the formation of nitric acid and nitrous acid ($pK_{a,HNO_2} = 3.35$).[26]

Nevertheless, the contribution of reaction R6 to the production of a nitrate ion appears a negligible one in control experiments, impinging only NO_2 onto the microdroplets,[15] which also discard any direct contribution of NO_2 alone to the formation 4-nitroctaechol. In agreement with the previous observation, thin films of catechol exposed only to NO_2 in the dark did not display any reactivity.[59]

The molar yields in Figure 5 (with a maximum theorical value of 1) are calculated from the ratios of the increments of

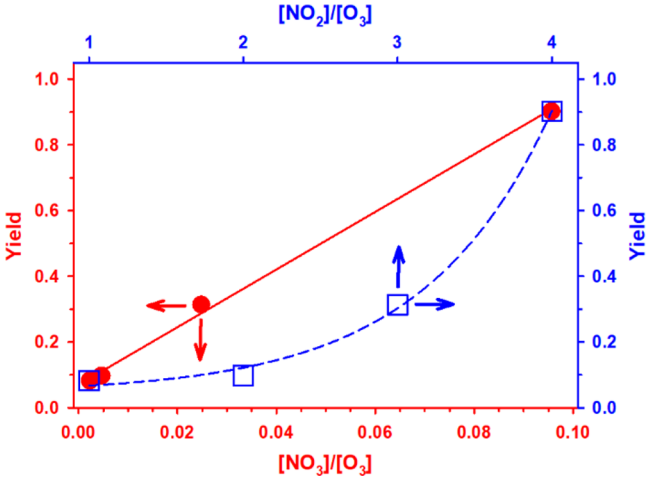

Figure 5. Molar yield of 4-nitrocatechol versus the ratio of (red solid circle) $[NO_3]$:$[O_3]$ and (blue square) $[NO_2]$:$[O_3]$. The red line corresponds to a linear fitting through the circles provided by the equation: yield = 0.0701 + 8.77 × $[NO_3]/[O_3]$, with coefficient of determination $r^2 = 0.998$. The blue dashed line through the squares is provided as a guide to the eye only.

4-nitrocatechol produced and interfacial catechol consumed (yield = Δ[4-nitrocatechol]/Δ[catechol]) and plotted against the $[NO_3]$:$[O_3]$ ratio using the left and bottom axes. For comparison, Figure 5 also displays the yields versus the ratio $[NO_2]$:$[O_3]$ in the top and right axes. The dependance of the yield of 4-nitrocatechol on $[NO_3]$:$[O_3]$ showed by the red solid line fitted through the circles in Figure 5 clearly demonstrates a direct linear dependance (which is not the case versus $[NO_2]$:$[O_3]$). The upper yield value in Figure 5, corresponding to a 4:1 ratio of $[NO_2]$:$[O_3]$, is 0.90 and within the center of the range (from 0.86 to 0.95) reported by Finewax et al.[14] Thus, a significant finding from these results is to report the changing yield of 4-nitrocatechol production per catechol consumed, which rises for highly polluted sites. In polluted sites the concentration of NO_2 is significant enough to produce NO_3 that outcompetes reactions with O_3 (high NO_3:O_3 ratios). Such conditions are dominant close to the point source of biomass burning plumes, in large smoke plumes that are dark enough to limit transmission of visible light and for combustion emissions rich in NO_x.

Proposed Reaction Mechanisms. Catechol (QH_2) is proposed to react with the mix of $[NO_2]$:$[O_3]$ by three competitive pathways on the surfaces of the aqueous microdroplets. In the first mechanism (reactions to the top of Scheme 1), electron transfer from QH_2 to NO_3 is thermodynamically favorable with a free energy change $\Delta G^{\circ}_{QH_2+NO_3} < 0$ under acidic conditions (pH < 7),[15] creating a radical cation ($QH_2^{\bullet+}$, $pK_a \approx -1.62$)[60] that deprotonates in picoseconds and NO_3^-. In more detail, based on the speciation of catechol ($pK_{a1} = 9.34$ and $pK_{a2} = 12.26$),[26,61] the undissociated molecule QH_2 represented in Scheme 1 should be the most abundant to react with the impinging oxidant at the pH of any atmospheric water.[15] Based on the definition of pH as chemical potential, both phases in equilibrium (interfacial and bulk water) have the same pH.[24] Thus, the referenced pK_a values for aerosolized solutes are of qualitative relevance here to the mechanisms discussed. The redox potential of catechol, $E_{H_2Q^{\bullet+}/H2Q} \geq 0.562$ V for pH ≤ 7,[15] together with the potential of nitrate radical, $E_{NO_3/NO_3^-} = 2.466$ V,[62] allow the calculation of the overall redox potential change for electron transfer from QH_2 to NO_3, $\Delta E_{NO_3} = E_{NO_3/NO_3^-} - E_{QH_2^{\bullet+}/QH_2} = 1.904$ V.[15] Therefore, the free energy change associated with the one electron transfer from QH_2 to NO_3, $\Delta G^{\circ}_{QH_2+NO_3} = -nF\,\Delta E_{NO_3} = -1 \times 96.485$ kJ mol^{-1} V^{-1} × 1.904 V = −183.7 kJ mol^{-1},[15] indicates the reaction proceeds spontaneously and is 4-times more favorable than for the equivalent reaction $QH_2 + O_3$.[15]

Nitrate ion resulting from electron transfer instantly accepts the proton released from $QH_2^{\bullet+}$, resulting in a semiquinone radical ($QH^{\bullet}$) with a $pK_{a,QH^{\bullet}} = 5$.[63] Finally, the attack of NO_2 to $QH^{\bullet}$ proceeds through an intermediate that after recovering aromaticity yields 4-nitrocatechol. Such a mechanism is experimentally supported by the enhancement in the production of 4-nitrocatechol at pH 4, when the undissociated fraction of $QH^{\bullet}$ is larger than for experiments at pH 5.[15]

The second operative mechanism (reactions in the middle of Scheme 1) consists of the electrophilic addition of NO_3 to catechol, which occurs at C_3 as the most activated ring position. The resulting cyclohexadienyl radical ($^{\bullet}C_6H_6O_5N_1$) intermediate 1 has been described in the hydroxylation of catechol by $HO^{\bullet}$ at the air-water interface.[18] Finally, recombination between adsorbed NO_2 and $^{\bullet}C_6H_6O_5N_1$ forms a closed shell intermediate 2 with general formula $C_6H_6O_7N_2$ that rearranges into 4-nitrocatechol eliminating HNO_3. The main support for this mechanism arises from the experimental observation that nitration of non-aromatic muconic acid should proceed by addition of NO_3 through a

https://doi.org/10.1021/acsestair.3c00001
ACS EST Air 2024, 1, 80−91

Scheme 1. Proposed Reaction Mechanisms: Mechanism 1: Electron and Proton Transfer Mechanism of 4-Nitrocatechol Formation at the Air−Water Interface. Mechanism 2: Nitrate Radical Electrophilic Addition Mechanism of 4-Nitrocatechol Formation at the Air−Water Interface. Mechanism 3: Direct Attack by NO_2^+ Produced from N_2O_5

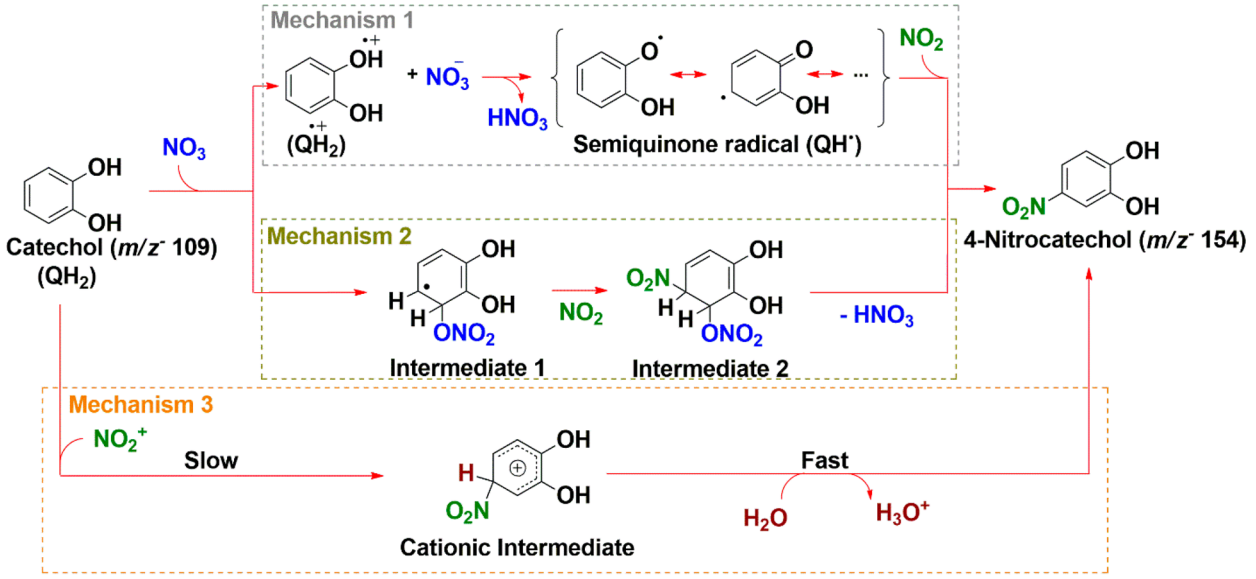

similar allyl radical to the cyclohexadienyl radical, but cannot proceed by the first mechanism introduced.[15]

Recycling of HNO_3 into NO_3 in mechanisms 1 and 2 above can be facilitated by in situ produced $HO^\bullet$ (e.g., from reaction R4) by reaction R7:

$$HNO_3 + HO^\bullet \rightarrow NO_3 + H_2O \quad \text{(R7)}$$

with the participation of water clusters that stabilize a $HNO_3\cdots$ OH complex for coupled proton−electron transfer to proceed.[64] This recycling mechanism of NO_3 should contribute to oxidize catechol on the microdroplets' surface more favorably at low pH.

The third mechanism for 4-nitrocatechol formation (bottom reactions in Scheme 1) involves the direct action of N_2O_5 under the acidic conditions (pH ≤ 4) governing atmospheric aerosol particles. The remaining 80% of the N_2O_5 reaching the microdroplets' surface that does not participate in reaction R5 can dissociate by reaction R8:

$$N_2O_5(ads) \rightleftharpoons NO_3^-(aq) + NO_2^+(aq) \quad \text{(R8)}$$

forming a nitronium ion (NO_2^+),[50,65] a strong electrophile. Thus, the third mechanism proceeds by electrophilic nitration facilitated by the attack of NO_2^+ to the aromatic ring,[66] which is more favorable at the low pH of atmospheric aerosols.[27] In this case, a Wheland cationic intermediate is generated in a slow first step, followed by fast loss of H^+ to produce 4-nitrocatechol.[67] Nonradical nitration by HNO_2/NO_2^- (e.g., the ion count at m/z^- 46 for NO_2^- from reaction R6 is insignificant even for $[NO_2]$:$[O_3]$ = 4:1) does not contribute to the observed production of 4-nitrocatechol in this work.

The conversion of catechol into 4-nitrocatechol depends linearly on the ratio of $[NO_3]$:$[O_3]$ rather than on $[NO_2]$:$[O_3]$, as displayed in Figure 5. Indeed, these mechanisms become more efficient at higher $[NO_3]$:$[O_3]$, which in turn growth as the ratio $[NO_2]$:$[O_3]$ increases from 1:1 to 4:1, as demonstrated by the yield behavior in Figure 5 and by the linear growth of the ion count at m/z^- 62 for NO_3^- in Figure 4. A simple kinetics comparison of the previous heterogeneous reaction rates demonstrates that only 4.2 ppqv $NO_3(g)$ ($[NO_3]$ = 1.0 × 10^5 molecules cm^{-3}) would compete for surface catechol with typical ambient level of 40 ppbv $O_3(g)$ ($[O_3]$ = 9.55 × 10^{11} molecules cm^{-3}). Moreover, as the level of NO_3 in wildfire plumes can be much higher (e.g., 7−20 pptv), the dark atmospheric oxidation of catechol on particulate matter is dominated by this radical, as depicted in Scheme 1.

Both the probability of electron transfer (Pathway 1) and NO_3 addition to the ring (Pathway 2) increase for a larger $[NO_3]$. In consequence, the initial steps of these pathways may not exhibit considerable differences for an increasing $[NO_3]$:$[O_3]$ ratio in this work. However, it must be noted that thermodynamically favorable electron transfer should proceed in a simpler way than the rate-limiting first step of NO_3 electrophilic substitution to create intermediate 1 in Scheme 1. Moreover, for the expected pH of biomass burning aerosol that can be as high as 5 due to the large presence of ammonia,[68] mechanism 3 in Scheme 1 should be the less competitive one across the $[NO_2]$:$[O_3]$ range studied.

The concerted production of dihydroxymaleic acid is tentatively proposed to start by the addition of NO_3 to 4-nitrocatechol (Scheme S1, Supporting Information). Such a process is similar to that depicted in a nitration pathway by Salvador et al.[6] based on a master chemical mechanism. We propose that the cyclohexadienyl radical created readily incorporates dioxygen in the C_4 and C_6 positions, resulting in a new carbon centered radical in C_3. A peroxide is formed by the O_2 addition to C_3 generating an unstable peroxide intermediate that causes the fast cleavage of the ring to form dihydroxymaleic acid.

Evaluation of Reactive Uptake of NO_3 by Catechol at the Air−Water Interface. The heterogeneous conversion of catechol in 4-nitrocatechol can proceed by the mechanisms listed above on the surface of atmospheric aerosol particles, cloudwater, and fog water that undergo NO_3 uptake. The reactive uptake coefficient of NO_3 (ν_{NO_3}) by catechol on the microdroplets' surface is evaluated next versus its value on pure water. Present experiments demonstrate that the loss of

https://doi.org/10.1021/acsestair.3c00001
ACS EST Air 2024, 1, 80−91

catechol in the continuous flow-through reactor is not limited by diffusion, as the molecules of catechol are quickly replenished to the interface from the underneath slab in the microdroplets in shorter time scales than the oxidation reaction. The mixing time scale, given by diffusion of the oxidizer into the outermost layer (τ_{d,NO_3} = 17 ns) and of catechol ($\tau_{d,catechol}$ = 25 ns) from the underneath layer, can be estimated for the three-dimensional volume ($\Delta x = \Delta y = \Delta z$) in the microdroplets with eq 2,[69]

$$\tau_d = \frac{\delta^2}{6D_i} \quad (2)$$

for a length of the underneath slab equivalent to the interface thickness (δ = 10 nm = 1 × 10^{-6} cm)[15,18,23] and the diffusion coefficient (D_i) of gaseous NO_3 (1 × 10^{-5} cm^2 s^{-1})[70] and catechol (6.61 × 10^{-6} cm^2 s^{-1})[71] in water. Therefore, the oxidation time scale (e.g., $\tau_c \approx 0.16$ μs) is not limited by the mixing time scale in the surrounding of the microdroplet surface slab.

Considering (1) a contact time, $\tau_c \approx 0.16 \times 10^{-6}$ s for the reaction studied in this setup; (2) δ = 1 × 10^{-6} cm for the microdroplets; (3) the mean molecular speed of NO_3(g) at 298 K, ν_{NO_3} = 3.42 × 10^4 cm s^{-1}; and (4) the dimensionless Henry's law constant for NO_3 in water, H_{O,NO_3} = 0.204 (at 298 K); it is possible to estimate a reasonable γ_{NO_3} by catechol on the surface of aqueous (10 μm diameter) microdroplets exposed to the impinging $[NO_3]_{eff}$ as done before for O_3:[18] $\gamma_{NO_3} = (4\delta H_{0,NO_3})/(\nu_{NO_3}\tau_c) = 1.5 \times 10^{-4}$. By definition γ_{NO_3} values should remain constant for a low range of oxidizer concentration, as explained before for the oxidation of catechol films by O_3 at fixed relative humidity.[21] This γ_{NO_3} value matches well with that measured for NO_3(g) in pure water at pH 7 that remains unchanged at pH 6 and 5.[45] Indeed, the fast oxidation of catechol studied occurs under conditions in which the reactive uptake of NO_3(g) can occur ~3× faster than the determined τ_c for the reaction of iodide with O_3 in the thin interface of microdroplets in the same OESI-MS setup.[23]

The observation that NO_2 alone did not induce oxidation during τ_c in our setup can be explained by comparing the oxidizing potentials given by the product of the uptake coefficients and the effective concentrations. The uptake coefficient of NO_2 by surface-adsorbed catechol on NaCl, γ_{NO_2} = 7 × 10^{-6} (at 30% RH).[72] Moreover, the theoretical unreacted $[NO_2]_{unreacted}$ after dilution with the nebulizer that reaches the surface of microdroplets for the experiments in Figure 4 should be in the range from 2.4 × 10^{12} to 5.1 × 10^{13} molecules cm^{-3}. These unreacted NO_2 concentrations are 1.3 × 10^4 to 6.9 × 10^2 times larger than the corresponding $[NO_3]_{eff}$, respectively. However, the oxidizing potential of NO_2 ($[NO_2]_{unreacted} \times \gamma_{NO_2}$) falls in the range from 2.7 × 10^4 to 1.1 × 10^7, which are of ≥2.9 × 10^5 times smaller than for the oxidizing potential of NO_3 ($[NO_3]_{eff} \times \gamma_{NO_3}$).

Based on the ratio of the presently estimated γ_{NO_3} to the reported reactive uptake for O_3 at 90% relative humidity, γ_{O_3},[21] $\gamma_{NO_3}/\gamma_{O_3}$ = 1.5 × 10^{-4}/1.6 × 10^{-5} = 9.4, nitration is considerably more efficient than ozonolysis in terms of reactive uptake. Moreover, NO_3 driven chemistry becomes clearly dominant given the much larger reactivity of this radical vs O_3[16,17] when appropriate $[O_3]$ and $[NO_2]$ ratios are used. Therefore, the recommendation of using $[NO_2]$:$[O_3]$ of 2:1 or higher should serve as a practical way to suppress ozonolysis and monitor only nitration during these interfacial reactions of catechol.

The previous recommendation is based on results from our flow-through reactor under an ultrafast (fixed) contact time. However, the branching ratio of ozonolysis to nitration is better described to vary with the ratio of output $[O_3]$ to the effective $[NO_3]$ (reported in the right hand-side column of Table 1) that together with the respective rate constants determine the fraction of catechol reacting with O_3 and NO_3 (e.g., for methoxyphenols $k_{PhOH+O_3}/k_{PhOH+NO_3} \leq 10^{-6}$ in the gas phase).[16,17] However, the ratio $[NO_3]$:$[O_3]$ is not constant for a fixed $[NO_2]$:$[O_3]$ ratio in other reactors, e.g., environmental chambers with longer reaction and residence times than our setup have been thoughtfully used to compare the competitive reactivity of monoterpenes with O_3 and NO_3.[73]

Environmental Implications. Catechol emitted during biomass burning and combustion processes favorably partitions to the surface of atmospheric particles, where it undergoes ultrafast reactions with NO_3 and N_2O_5 during the night to form 4-nitrocatechol. The mechanisms presented for the formation of 4-nitrocatechol at variable concentration ratios of O_3 and NO_2 justify why this molecule can be taken as a ubiquitous tracer for biomass burning secondary organic aerosols (SOA). Furthermore, nitro-aromatics behave as more hydrophobic and toxic molecules than the precursor aromatics,[74] raising human health concerns for exposed populations.

The generation of 4-nitrocatechol demonstrates a path for aromatic hydrocarbon pollutants to undergo a bathochromic shift, increasing the absorptivity of atmospheric particles. The presence of molecules such as 4-nitrocatechol in atmospheric brown carbon not only affects the radiative forcing of SOA,[7,8] but also turn the complex mixture more susceptible to photolysis[75] during daytime. In this context, the absorption of 4-nitrocatechol is lost by photobleaching during hydroxylation and fragmentation reactions.[75] Thus, multifunctional carboxylic acids[18,19] and oligomers[76] can be formed from this nitroaromatic compound, while the pH of particles drops. Furthermore, as the pH becomes more acidic, the production of 4-nitrocatechol in the presented mechanisms of this work is enhanced, maximizing the production of this chromophore in particle matter.[15]

The experiments in Table 1 measured the production of 4-nitrocatechol from the oxidation of catechol by O_3 with varying concentrations of NO_2 added. In other words, to compare the reactivity of catechol for a range of $[NO_2]$, the input of catechol (from the partitioning of 22.44 ppbv) and O_3 are fixed first, allowing the concentration of products and of NO_2 to vary. While several of the precursor concentrations of NO_2 and O_3 used in this study can be considered high, the yields of 4-nitrocatechol reported are atmospherically relevant in terms of the ratios of $[NO_2]$ and $[O_3]$ explored. Although using higher oxidizer concentrations than in the troposphere can produce high yields that may less likely represent radical fates, the ratios of $[NO_2]$:$[O_3]$ experimentally covered (including 0:1, 1:1, 1:2, 1:3, and 1:4) represent an atmospherically relevant range of conditions that span from pristine (O_3 dominated) to polluted locations (NO_2 dominated). Thus, the results of how catechol reacts when exposed to relevant oxidizer ratios of $[NO_2]$ and $[O_3]$ from biomass burning and

https://doi.org/10.1021/acsestair.3c00001
ACS EST Air 2024, 1, 80−91

combustion emissions are informative for the real atmosphere. The related biomass burning probe nitroguaicol exhibited an apparent drop of the reactive uptake of oxidizer from ~2.8 × 10^{-2} to ~1.5 × 10^{-2} (under dry conditions) for increasing NO_3 concentration from ~3 × 10^9 to 2 × 10^{10} molecules cm^{-3}.[77] The same type of dependance was observed for the reactive uptake of $HO^•$ radical by nitroguaicol.[78] Thus, it will be important to assess in the future if the NO_3 reactive uptake rates by the catechol surface at fixed relative humidities decrease as the $[NO_3]$ increase. Surface catechol should react during nighttime with 15 pptv of NO_3(g) with a lifetime of ~2.6 min (Supporting Information), indicating the efficient production of 4-nitrocatechol proceeds with a yield approaching 0.9 in the proximity to a biomass burning plume.

Spontaneous electron and proton transfers at the interface of water and air are key to initiating the chemistry that proceeds through a semiquinone radical intermediate. Alternatively, electrophilic aromatic substitution via a cyclohexadienyl radical intermediate is also a viable path for nitroaromatics' production. Thus, upon attack of NO_2 to either intermediate (semiquinone or cyclohexadienyl radicals), 4-nitrocatechol is generated together with HNO_3. Once generated, up to 68% of 4-nitrocatechol preferentially continues in the particle phase.[14] An independent reactivity channel that should operate favorably for acidic aerosol particles is provided by adsorbed N_2O_5 that generates the strong electrophilic nitronium ion capable of inducing the direct nitration of catechol. The results of this work demonstrate the importance of using appropriate ratios of $[NO_2]$:$[O_3]$ ≥ 2:1 in laboratory experiments studying the nitration mechanism of phenolic compounds such as catechol to prevent complications with competing ozonolysis reactions at higher concentration ratios. Similarly, Draper et al. reported a higher production of nitro products from monoterpenes when increasing the ratio NO_2:O_3.[73] The use of alternative systems could assist future kinetic measurements to determine concentration changes and uptake coefficients of reactive species on particles, which can be applied for the accurate estimation of lifetimes under multiple atmospheric conditions.

■ ASSOCIATED CONTENT

Supporting Information

The Supporting Information is available free of charge at https://pubs.acs.org/doi/10.1021/acsestair.3c00001.

Additional discussion with the lifetime calculation, and Scheme S1 for the proposed dihydroxymaleic acid formation (PDF)

■ AUTHOR INFORMATION

Corresponding Author

Marcelo I. Guzman − *Department of Chemistry, University of Kentucky, Lexington, Kentucky 40506, United States;* orcid.org/0000-0002-6730-7766; Phone: (859)323-2892; Email: marcelo.guzman@uky.edu

Authors

Md Sohel Rana − *Department of Chemistry, University of Kentucky, Lexington, Kentucky 40506, United States*

Seth T. Bradley − *Department of Chemistry, University of Kentucky, Lexington, Kentucky 40506, United States*

Complete contact information is available at: https://pubs.acs.org/10.1021/acsestair.3c00001

Notes

The authors declare no competing financial interest.

■ ACKNOWLEDGMENTS

Funding from the U.S.A. National Science Foundation (NSF) under Award 1903744 to M.I.G. is acknowledged. S.T.B. acknowledges support from a University of Kentucky NSF Research Traineeship Fellowship supported by NSF under Award 1922694.

■ ABBREVIATIONS

$E_{H_2Q^{•+}/H_2Q}$, redox potential for the reduction of catechol to radical cations; F, Faraday constant; $H_{0,i}$, Henry's law constant of species i; $HO^•$, hydroxyl radical; HNO_2, nitrous acid; HNO_3, nitric acid; $I_{m/z}$, ion count at value m/z^-; m/z^-, mass-to-charge ratio of anion; MS, mass spectrometry; MW, molecular weight; n, number of electrons transferred; NO_3, nitrate radical; NO_3^-, nitrate ion; NO_2, nitrogen dioxide; N_2O_5, dinitrogen pentoxide; O_3, ozone; OESI, online electrospray ionization; PDA, photodiode array; P_{NO_3}, NO_3 production rate; ppbv, parts per billion by volume; pptv, parts per trillion by volume; QH_2, undissociated form of catechol; $QH_2^{•+}$, radical cation of catechol; $QH^•$, semiquinone radical of catechol; SOA, secondary organic aerosol; τ_c, contact time; UHP, ultrahigh purity; ΔE, change of redox potential; $\Delta G^\circ_{QH_2+NO_3}$, free energy change for electron transfer of catechol to nitrate radical; ν_{NO_3}, reactive uptake coefficient of NO_3; λ, wavelength

■ REFERENCES

(1) Henze, D.; Seinfeld, J.; Ng, N.; Kroll, J.; Fu, T.-M.; Jacob, D. J.; Heald, C. Global modeling of secondary organic aerosol formation from aromatic hydrocarbons: high-vs. low-yield pathways. *Atmos. Chem. Phys.* **2008**, *8* (9), 2405−2420.

(2) Schauer, J. J.; Kleeman, M. J.; Cass, G. R.; Simoneit, B. R. T. Measurement of emissions from air pollution sources. 3. C1−C29 organic compounds from fireplace combustion of wood. *Environ. Sci. Technol.* **2001**, *35* (9), 1716−1728.

(3) Pillar-Little, E. A.; Guzman, M. I. An overview of dynamic heterogeneous oxidations in the troposphere. *Environments* **2018**, *5* (9), 104.

(4) Li, M.; Wang, X.; Lu, C.; Li, R.; Zhang, J.; Dong, S.; Yang, L.; Xue, L.; Chen, J.; Wang, W. Nitrated phenols and the phenolic precursors in the atmosphere in urban Jinan, China. *Sci. Total Environ.* **2020**, *714*, No. 136760.

(5) Wang, Y.; Hu, M.; Wang, Y.; Zheng, J.; Shang, D.; Yang, Y.; Liu, Y.; Li, X.; Tang, R.; Zhu, W.; Du, Z.; Wu, Y.; Guo, S.; Wu, Z.; Lou, S.; Hallquist, M.; Yu, J. Z. The formation of nitro-aromatic compounds under high NOx and anthropogenic VOC conditions in urban Beijing, China. *Atmos. Chem. Phys.* **2019**, *19* (11), 7649−7665.

(6) Salvador, C. M. G.; Tang, R.; Priestley, M.; Li, L.; Tsiligiannis, E.; Le Breton, M.; Zhu, W.; Zeng, L.; Wang, H.; Yu, Y.; Hu, M.; Guo, S.; Hallquist, M. Ambient nitro-aromatic compounds − biomass burning versus secondary formation in rural China. *Atmos. Chem. Phys.* **2021**, *21* (3), 1389−1406.

(7) Laskin, A.; Laskin, J.; Nizkorodov, S. A. Chemistry of atmospheric brown carbon. *Chem. Rev.* **2015**, *115* (10), 4335−82.

(8) Li, C.; He, Q.; Hettiyadura, A. P. S.; Käfer, U.; Shmul, G.; Meidan, D.; Zimmermann, R.; Brown, S. S.; George, C.; Laskin, A.; Rudich, Y. Formation of secondary brown carbon in biomass burning aerosol proxies through NO_3 radical reactions. *Environ. Sci. Technol.* **2020**, *54* (3), 1395−1405.

(9) Iinuma, Y.; Böge, O.; Gräfe, R.; Herrmann, H. Methyl-nitrocatechols: Atmospheric tracer compounds for biomass burning secondary organic aerosols. *Environ. Sci. Technol.* **2010**, *44* (22), 8453−8459.

(10) Zhang, Q.; Shen, Z.; Zhang, L.; Zeng, Y.; Ning, Z.; Zhang, T.; Lei, Y.; Wang, Q.; Li, G.; Sun, J.; Westerdahl, D.; Xu, H.; Cao, J. Investigation of primary and secondary particulate brown carbon in two chinese cities of Xi'an and Hong Kong in wintertime. *Environ. Sci. Technol.* **2020**, *54* (7), 3803−3813.
(11) Mohr, C.; Lopez-Hilfiker, F. D.; Zotter, P.; Prévôt, A. S. H.; Xu, L.; Ng, N. L.; Herndon, S. C.; Williams, L. R.; Franklin, J. P.; Zahniser, M. S.; Worsnop, D. R.; Knighton, W. B.; Aiken, A. C.; Gorkowski, K. J.; Dubey, M. K.; Allan, J. D.; Thornton, J. A. Contribution of nitrated phenols to wood burning brown carbon light absorption in detling, United Kingdom during winter time. *Environ. Sci. Technol.* **2013**, *47* (12), 6316−6324.
(12) Zeng, L.; Zhang, A.; Wang, Y.; Wagner, N. L.; Katich, J. M.; Schwarz, J. P.; Schill, G. P.; Brock, C.; Froyd, K. D.; Murphy, D. M.; Williamson, C. J.; Kupc, A.; Scheuer, E.; Dibb, J.; Weber, R. J. Global measurements of brown carbon and estimated direct radiative effects. *Geophys. Res. Lett.* **2020**, *47* (13), No. e2020GL088747.
(13) Barzaghi, P.; Herrmann, H. Kinetics and mechanisms of reactions of the nitrate radical (NO_3) with substituted phenols in aqueous solution. *Phys. Chem. Chem. Phys* **2004**, *6* (23), 5379−5388.
(14) Finewax, Z.; de Gouw, J. A.; Ziemann, P. J. Identification and quantification of 4-nitrocatechol formed from OH and NO_3 radical-initiated reactions of catechol in air in the presence of NO_X: Implications for secondary organic aerosol formation from biomass burning. *Environ. Sci. Technol.* **2018**, *52* (4), 1981−1989.
(15) Rana, M. S.; Guzman, M. I. Oxidation of catechols at the air−water interface by nitrate radicals. *Environ. Sci. Technol.* **2022**, *56* (22), 15437−15448.
(16) Yang, B.; Zhang, H.; Wang, Y.; Zhang, P.; Shu, J.; Sun, W.; Ma, P. Experimental and theoretical studies on gas-phase reactions of NO_3 radicals with three methoxyphenols: Guaiacol, creosol, and syringol. *Atmos. Environ.* **2016**, *125*, 243−251.
(17) Zein, A. E.; Coeur, C.; Obeid, E.; Lauraguais, A.; Fagniez, T. Reaction kinetics of catechol (1,2-benzenediol) and guaiacol (2-methoxyphenol) with ozone. *J. Phys. Chem. A* **2015**, *119* (26), 6759−6765.
(18) Pillar-Little, E. A.; Camm, R. C.; Guzman, M. I. Catechol oxidation by ozone and hydroxyl radicals at the air−water interface. *Environ. Sci. Technol.* **2014**, *48* (24), 14352−14360.
(19) Pillar-Little, E. A.; Guzman, M. I. Oxidation of substituted catechols at the air−water interface: Production of carboxylic acids, quinones, and polyphenols. *Environ. Sci. Technol.* **2017**, *51* (9), 4951−4959.
(20) Pillar-Little, E. A.; Zhou, R.; Guzman, M. I. Heterogeneous oxidation of catechol. *J. Phys. Chem. A* **2015**, *119* (41), 10349−10359.
(21) Guzman, M. I.; Pillar-Little, E. A.; Eugene, A. J. Interfacial oxidative oligomerization of catechol. *ACS Omega* **2022**, *7* (40), 36009−36016.
(22) Guzman, M. I.; Athalye, R. R.; Rodriguez, J. M. Concentration effects and ion properties controlling the fractionation of halides during aerosol formation. *J. Phys. Chem. A* **2012**, *116* (22), 5428−5435.
(23) Pillar-Little, E. A.; Guzman, M. I.; Rodriguez, J. M. Conversion of iodide to hypoiodous acid and iodine in aqueous microdroplets exposed to ozone. *Environ. Sci. Technol.* **2013**, *47* (19), 10971−10979.
(24) Eugene, A. J.; Pillar-Little, E. A.; Colussi, A. J.; Guzman, M. I. Enhanced acidity of acetic and pyruvic acids on the surface of water. *Langmuir* **2018**, *34* (31), 9307−9313.
(25) Veres, P.; Roberts, J. M.; Burling, I. R.; Warneke, C.; de Gouw, J.; Yokelson, R. J. Measurements of gas-phase inorganic and organic acids from biomass fires by negative-ion proton-transfer chemical-ionization mass spectrometry. *J. Geophys. Res. -Atmos.* **2010**, *115* (23), No. D23302.
(26) Haynes, W. M., Ed. *CRC Handbook of Chemistry and Physics*, 93rd ed.; CRC Press/Taylor and Francis: Boca Raton, FL, 2013; p 2664.
(27) Pye, H. O. T.; Nenes, A.; Alexander, B.; Ault, A. P.; Barth, M. C.; Clegg, S. L.; Collett, J. L., Jr; Fahey, K. M.; Hennigan, C. J.; Herrmann, H.; Kanakidou, M.; Kelly, J. T.; Ku, I. T.; McNeill, V. F.; Riemer, N.; Schaefer, T.; Shi, G.; Tilgner, A.; Walker, J. T.; Wang, T.; Weber, R.; Xing, J.; Zaveri, R. A.; Zuend, A. The acidity of atmospheric particles and clouds. *Atmos. Chem. Phys.* **2020**, *20* (8), 4809−4888.
(28) Rana, M. S.; Guzman, M. I. Oxidation of phenolic aldehydes by ozone and hydroxyl radicals at the air−water interface. *J. Phys. Chem. A* **2020**, *124* (42), 8822−8833.
(29) Rana, M. S.; Guzman, M. I. Surface oxidation of phenolic aldehydes: Fragmentation, functionalization, and coupling reactions. *J. Phys. Chem. A* **2022**, *126* (37), 6502−6516.
(30) Sander, S. P.; Friedl, R. R.; Barker, J. R.; Golden, D. M.; Kurylo, M. J.; Wine, P. H.; Abbatt, J.; Burkholder, J. B.; Kolb, C. E.; Moortgat, G. K.; Huie, R. E.; Orkin, V. L. *Chemical Kinetics and Photochemical Data for Use in Atmospheric Studies: Evaluation Number 17*; Jet Propulsion Laboratory, National Aeronautics and Space Administration: Pasadena, CA, 2009.
(31) Brown, S. S.; Stutz, J. Nighttime radical observations and chemistry. *Chem. Soc. Rev.* **2012**, *41* (19), 6405−6447.
(32) Wood, E. C.; Wooldridge, P. J.; Freese, J. H.; Albrecht, T.; Cohen, R. C. Prototype for in situ detection of atmospheric NO_3 and N_2O_5 via laser-induced fluorescence. *Environ. Sci. Technol.* **2003**, *37* (24), 5732−5738.
(33) Dubé, W. P.; Brown, S. S.; Osthoff, H. D.; Nunley, M. R.; Ciciora, S. J.; Paris, M. W.; McLaughlin, R. J.; Ravishankara, A. R. Aircraft instrument for simultaneous, in situ measurement of NO_3 and N_2O_5 via pulsed cavity ring-down spectroscopy. *Rev. Sci. Instrum.* **2006**, *77* (3), No. 034101.
(34) Lambe, A. T.; Wood, E. C.; Krechmer, J. E.; Majluf, F.; Williams, L. R.; Croteau, P. L.; Cirtog, M.; Féron, A.; Petit, J. E.; Albinet, A.; Jimenez, J. L.; Peng, Z. Nitrate radical generation via continuous generation of dinitrogen pentoxide in a laminar flow reactor coupled to an oxidation flow reactor. *Atmos. Meas. Tech.* **2020**, *13* (5), 2397−2411.
(35) Fry, J. L.; Kiendler-Scharr, A.; Rollins, A. W.; Wooldridge, P. J.; Brown, S. S.; Fuchs, H.; Dubé, W.; Mensah, A.; dal Maso, M.; Tillmann, R.; Dorn, H. P.; Brauers, T.; Cohen, R. C. Organic nitrate and secondary organic aerosol yield from NO_3 oxidation of β-pinene evaluated using a gas-phase kinetics/aerosol partitioning model. *Atmos. Chem. Phys.* **2009**, *9* (4), 1431−1449.
(36) Ren, Y.; Zhou, L.; Mellouki, A.; Daële, V.; Idir, M.; Brown, S. S.; Ruscic, B.; Paton, R. S.; McGillen, M. R.; Ravishankara, A. R. Reactions of NO_3 with aromatic aldehydes: gas-phase kinetics and insights into the mechanism of the reaction. *Atmos. Chem. Phys.* **2021**, *21* (17), 13537−13551.
(37) Dewald, P.; Liebmann, J. M.; Friedrich, N.; Shenolikar, J.; Schuladen, J.; Rohrer, F.; Reimer, D.; Tillmann, R.; Novelli, A.; Cho, C.; Xu, K.; Holzinger, R.; Bernard, F.; Zhou, L.; Mellouki, W.; Brown, S. S.; Fuchs, H.; Lelieveld, J.; Crowley, J. N. Evolution of NO_3 reactivity during the oxidation of isoprene. *Atmos. Chem. Phys.* **2020**, *20* (17), 10459−10475.
(38) Akther, T.; Ahmed, M.; Shohel, M.; Ferdousi, F. K.; Salam, A. Particulate matters and gaseous pollutants in indoor environment and Association of ultra-fine particulate matters (PM_1) with lung function. *Environ. Sci. Pollut. Res.* **2019**, *26* (6), 5475−5484.
(39) Zhang, Y.; Tang, L.; Sun, Y.; Favez, O.; Canonaco, F.; Albinet, A.; Couvidat, F.; Liu, D.; Jayne, J. T.; Wang, Z.; Croteau, P. L.; Canagaratna, M. R.; Zhou, H.-c.; Prévôt, A. S. H.; Worsnop, D. R. Limited formation of isoprene epoxydiols-derived secondary organic aerosol under NOx-rich environments in Eastern China. *Geophys. Res. Lett.* **2017**, *44* (4), 2035−2043.
(40) Huang, G.; Liu, Y.; Shao, M.; Li, Y.; Chen, Q.; Zheng, Y.; Wu, Z.; Liu, Y.; Wu, Y.; Hu, M.; Li, X.; Lu, S.; Wang, C.; Liu, J.; Zheng, M.; Zhu, T. Potentially important contribution of gas-phase oxidation of naphthalene and methylnaphthalene to secondary organic aerosol during haze events in Beijing. *Environ. Sci. Technol.* **2019**, *53*, 1235−1244.
(41) Wang, Y.; Pavuluri, C. M.; Fu, P.; Li, P.; Dong, Z.; Xu, Z.; Ren, H.; Fan, Y.; Li, L.; Zhang, Y.-L.; Liu, C.-Q. Characterization of

https://doi.org/10.1021/acsestair.3c00001
ACS EST Air 2024, 1, 80−91

secondary organic aerosol tracers over Tianjin, North China during summer to autumn. *ACS Earth Space Chem.* **2019**, *3*, 2339−2352.
(42) Kim, Y.; Kim, H.; Kang, H.; de Foy, B.; Zhang, Q. Impacts of secondary aerosol formation and long range transport on severe haze during the winter of 2017 in the Seoul metropolitan area. *Sci. Total Environ.* **2022**, *804*, No. 149984.
(43) Ding, J.; Dai, Q.; Zhang, Y.; Xu, J.; Huangfu, Y.; Feng, Y. Air humidity affects secondary aerosol formation in different pathways. *Sci. Total Environ.* **2021**, *759*, No. 143540.
(44) Decker, Z. C. J.; Zarzana, K. J.; Coggon, M.; Min, K.-E.; Pollack, I.; Ryerson, T. B.; Peischl, J.; Edwards, P.; Dubé, W. P.; Markovic, M. Z.; Roberts, J. M.; Veres, P. R.; Graus, M.; Warneke, C.; de Gouw, J.; Hatch, L. E.; Barsanti, K. C.; Brown, S. S. Nighttime chemical transformation in biomass burning plumes: A box model analysis initialized with aircraft observations. *Environ. Sci. Technol.* **2019**, *53*, 2529−2538.
(45) Rudich, Y.; Talukdar, R. K.; Ravishankara, A. R.; Fox, R. W. Reactive uptake of NO_3 on pure water and ionic solutions. *J. Geophys. Res.* **1996**, *101* (D15), 21023−21031.
(46) Mentel, T. F.; Sohn, M.; Wahner, A. Nitrate effect in the heterogeneous hydrolysis of dinitrogen pentoxide on aqueous aerosols. *Phys. Chem. Chem. Phys.* **1999**, *1* (24), 5451−5457.
(47) Dean, J. A., Ed. In *Lange's Handbook of Chemistry*, 15th ed.; McGraw-Hill: New York, NY, 1999; p 1538.
(48) Hirshberg, B.; Rossich Molina, E.; Götz, A. W.; Hammerich, A. D.; Nathanson, G. M.; Bertram, T. H.; Johnson, M. A.; Gerber, R. B. N_2O_5 at water surfaces: binding forces, charge separation, energy accommodation and atmospheric implications. *Phys. Chem. Chem. Phys.* **2018**, *20* (26), 17961−17976.
(49) Mentel, T. F.; Bleilebens, D.; Wahner, A. A study of nighttime nitrogen oxide oxidation in a large reaction chamber—the fate of NO_2, N_2O_5, HNO_3, and O_3 at different humidities. *Atmos. Environ.* **1996**, *30* (23), 4007−4020.
(50) Schütze, M.; Herrmann, H. Determination of phase transfer parameters for the uptake of HNO_3, N_2O_5 and O_3 on single aqueous drops. *Phys. Chem. Chem. Phys.* **2002**, *4* (1), 60−67.
(51) Jin, Z.; Qian, L.; Shi, Y.; Fu, G.; Li, G.; Li, F. Quantifying major NOx sources of aerosol nitrate in Hangzhou, China, by using stable isotopes and a Bayesian isotope mixing model. *Atmos. Environ.* **2021**, *244*, No. 117979.
(52) Schütze, M.; Herrmann, H. Uptake of the NO_3 radical on aqueous surfaces. *J. Atmos. Chem.* **2005**, *52* (1), 1−18.
(53) Sander, R. Compilation of Henry's law constants (version 4.0) for water as solvent. *Atmos. Chem. Phys.* **2015**, *15* (8), 4399−4981.
(54) Galib, M.; Limmer, D. T. Reactive uptake of N_2O_5 by atmospheric aerosol is dominated by interfacial processes. *Science* **2021**, *371* (6532), 921.
(55) Badger, C. L.; Griffiths, P. T.; George, I.; Abbatt, J. P. D.; Cox, R. A. Reactive uptake of N_2O_5 by aerosol particles containing mixtures of humic acid and ammonium sulfate. *J. Phys. Chem. A* **2006**, *110* (21), 6986−6994.
(56) Mogili, P. K.; Kleiber, P. D.; Young, M. A.; Grassian, V. H. N_2O_5 hydrolysis on the components of mineral dust and sea salt aerosol: Comparison study in an environmental aerosol reaction chamber. *Atmos. Environ.* **2006**, *40* (38), 7401−7408.
(57) Chang, W. L.; Brown, S. S.; Stutz, J.; Middlebrook, A. M.; Bahreini, R.; Wagner, N. L.; Dubé, W. P.; Pollack, I. B.; Ryerson, T. B.; Riemer, N. Evaluating N_2O_5 heterogeneous hydrolysis parameterizations for CalNex 2010. *J. Geophys. Res. -Atmos.* **2016**, *121* (9), 5051−5070.
(58) Lee, Y. N.; Schwartz, S. E. Reaction kinetics of nitrogen dioxide with liquid water at low partial pressure. *J. Phys. Chem.* **1981**, *85* (7), 840−848.
(59) Nichols, B. R.; Rapa, C.; Costa, V.; Hinrichs, R. Z. Heterogeneous and photochemical reactions of solid benzophenone−catechol films with NO_2. *J. Phys. Chem. C* **2009**, *113* (6), 2111−2119.
(60) Steenken, S.; Neta, P. Properties of Phenoxyl Radicals. In *The Chemistry of Phenols*; Rappoport, Z., Ed.; John Wiley & Sons: New York, 2003; p 1000.
(61) Perrin, D. D., Dempsey, B., Serjeant, E. P., Eds. *pK_a Prediction for Organic Acids and Bases*, 1st ed.; Springer Netherlands: London, 1981; p 146.
(62) Armstrong, D. A.; Huie, R. E.; Koppenol, W. H.; Lymar, S. V.; Merényi, G.; Neta, P.; Ruscic, B.; Stanbury, D. M.; Steenken, S.; Wardman, P. Standard electrode potentials involving radicals in aqueous solution: inorganic radicals (IUPAC Technical Report). *Pure Appl. Chem.* **2015**, *87* (11-12), 1139−1150.
(63) Steenken, S.; O'Neill, P. Oxidative demethoxylation of methoxylated phenols and hydroxybenzoic acids by the hydroxyl radical. An in situ electron spin resonance, conductometric pulse radiolysis and product analysis study. *J. Phys. Chem.* **1977**, *81* (6), 505−508.
(64) Anglada, J. M.; Martins-Costa, M. T. C.; Francisco, J. S.; Ruiz-López, M. F. Reactivity of undissociated molecular nitric acid at the air−water interface. *J. Am. Chem. Soc.* **2021**, *143* (1), 453−462.
(65) Behnke, W.; George, C.; Scheer, V.; Zetzsch, C. Production and decay of $ClNO_2$ from the reaction of gaseous N_2O_5 with NaCl solution: Bulk and aerosol experiments. *J. Geophys. Res-Atmos.* **1997**, *102* (D3), 3795−3804.
(66) Taylor, R., Ed. *Electrophilic Aromatic Substitution*; Wiley: New York, 1990; p 530.
(67) Ridd, J. H.; Pletcher, D.; Qiao, X.; Pascal, R. A., Jr.; Bard, A. J.; Francis, G. W.; Szunyog, J.; Langstrom, B. Some unconventional pathways in aromatic nitration. *Acta Chem. Scand.* **1998**, *52* (1), 11−22.
(68) Nault, B. A.; Campuzano-Jost, P.; Day, D. A.; Guo, H.; Jo, D. S.; Handschy, A. V.; Pagonis, D.; Schroder, J. C.; Schueneman, M. K.; Cubison, M. J.; Dibb, J. E.; Hodzic, A.; Hu, W.; Palm, B. B.; Jimenez, J. L. Interferences with aerosol acidity quantification due to gas-phase ammonia uptake onto acidic sulfate filter samples. *Atmos. Meas. Tech.* **2020**, *13* (11), 6193−6213.
(69) Bird, R., Stewart, W., Lightfoot, E., Eds. *Transport Phenomena*, 2nd ed.; John Wiley and Sons: New York, 2002; p 905.
(70) Mallard, W. G.; Linstrom, P. J. *Standard Reference Database 69: The NIST Chemistry WebBook*; National Institute of Standards and Technology: Gaithersburg, MD, 2000; Vol. *2012*, http://webbook.nist.gov, accessed 2023/9/24.
(71) Sharma, L. R.; Kalia, R. K. Hydrodynamic voltammetry at the tubular graphite electrode. Determination of diffusion coefficients of aromatic amino and phenolic compounds. *J. Chem. Eng. Data* **1977**, *22* (1), 39−41.
(72) Woodill, L. A.; Hinrichs, R. Z. Heterogeneous reactions of surface-adsorbed catechol with nitrogen dioxide: substrate effects for tropospheric aerosol surrogates. *Phys. Chem. Chem. Phys.* **2010**, *12* (36), 10766−10774.
(73) Draper, D. C.; Farmer, D. K.; Desyaterik, Y.; Fry, J. L. A qualitative comparison of secondary organic aerosol yields and composition from ozonolysis of monoterpenes at varying concentrations of NO_2. *Atmos. Chem. Phys.* **2015**, *15* (21), 12267−12281.
(74) Wei, B.; Sun, J.; Mei, Q.; An, Z.; Wang, X.; He, M. Theoretical study on gas-phase reactions of nitrate radicals with methoxyphenols: Mechanism, kinetic and toxicity assessment. *Environ. Pollut.* **2018**, *243*, 1772−1780.
(75) Zhao, R.; Lee, A. K. Y.; Huang, L.; Li, X.; Yang, F.; Abbatt, J. P. D. Photochemical processing of aqueous atmospheric brown carbon. *Atmos. Chem. Phys.* **2015**, *15* (11), 6087−6100.
(76) Hems, R. F.; Abbatt, J. P. D. Aqueous phase photo-oxidation of brown carbon nitrophenols: Reaction kinetics, mechanism, and evolution of light absorption. *ACS Earth Space Chem.* **2018**, *2* (3), 225−234.
(77) Knopf, D. A.; Forrester, S. M.; Slade, J. H. Heterogeneous oxidation kinetics of organic biomass burning aerosol surrogates by O_3, NO_2, N_2O_5, and NO_3. *Phys. Chem. Chem. Phys.* **2011**, *13* (47), 21050−21062.

https://doi.org/10.1021/acsestair.3c00001
ACS EST Air 2024, 1, 80−91

(78) Slade, J. H.; Knopf, D. A. Heterogeneous OH oxidation of biomass burning organic aerosol surrogate compounds: assessment of volatilisation products and the role of OH concentration on the reactive uptake kinetics. *Phys. Chem. Chem. Phys.* **2013**, *15* (16), 5898−5915.

https://doi.org/10.1021/acsestair.3c00001
ACS EST Air 2024, 1, 80−91